Biomass Conversion and Biorefinery
https://doi.org/10.1007/s13399-023-05250-1

ORIGINAL ARTICLE

Phytosynthesis of silver nanoparticles using guarana (*Paullinia cupana* Kunth) leaf extract employing different routes: characterization and investigation of in vitro bioactivities

Alan Kelbis Oliveira Lima[1] · Ariane Pandolfo Silveira[2] · Renata Carvalho Silva[3] · Yasmin Alves Aires Machado[4] · Alyne Rodrigues de Araújo[5] · Sansara Sanny de Mendonça Araujo[5] · Italo Rennan Sousa Vieira[6] · Joabe Lima Araújo[1] · Lucas Carvalho dos Santos[7] · Klinger Antônio da França Rodrigues[4] · Sebastião William da Silva[8] · José Antônio de Aquino Ribeiro[9] · Clenilson Martins Rodrigues[9] · Mônica Pereira Garcia[1]

Received: 18 October 2023 / Revised: 10 December 2023 / Accepted: 23 December 2023

Abstract

The optimization techniques are fundamental to guarantee the stability of any preparation process and the quality of the nanostructures synthesized under ideal circumstances. In this sense, this study evaluates the potential of guarana leaf extract (*Paullinia cupana* Kunth—Sapindaceae) for the green synthesis of silver nanoparticles (AgNPs) using routes that employ different equipment/energy sources (autoclave, LED, microwave, sunlight, ultrasound, and water bath). The aqueous extract was characterized by high-performance liquid chromatography coupled with high-resolution mass spectrometry (UHPLC-HRMS/MS). The AgNPs were analyzed by UV/Vis spectroscopy, dynamic light scattering (DLS), zeta potential (ZP), Fourier transform infrared (FTIR), transmission electron microscopy (TEM) and their antibacterial, leishmanicidal and cytotoxic effects were evaluated in vitro. The results show the presence of phenolic acids, alkaloids, and flavonoids in the leaf extract, which was supported by the identification of their functional groups in the FTIR spectra. The AgNPs showed maximum absorption between 420 and 440 nm (UV/Vis), with a diameter below 100 nm (DLS) and 60 nm (TEM), spherical morphology and a surface charge above − 30 mV (ZP). The antibacterial test showed pronounced inhibition in the growth of *Escherichia coli*, *Pseudomonas aeruginosa* and *Staphylococcus aureus* bacteria. The leishmanicidal activity of AgNPs on *Leishmania (Leishmania) amazonensis* was more pronounced than that of the drug miltefosine while low cytotoxicity was reported on RAW 264.7 macrophages. With this, this study reports the possibility of using alternative routes for the sustainable synthesis of AgNPs from *Paullinia cupana* extract with considerable applications against pathogenic bacteria and opportunistic parasites.

Keywords AgNPs · Amazon · Antibacterial · Antileishmania · Metallic nanoparticles

✉ Alan Kelbis Oliveira Lima
kelbislima@gmail.com

[1] Nanobiotechnology Laboratory, Institute of Biological Sciences, University of Brasilia (UnB), Brasilia, DF 70910-900, Brazil

[2] Laboratory of Microscopy and Microanalysis, Institute of Biological Sciences, University of Brasilia (UnB), Brasília, DF 70910-900, Brazil

[3] Quality and Technology (INMETRO), National Institute of Metrology, Duque de Caxias, Rio de Janeiro, RJ 25250-020, Brazil

[4] Laboratory of Infectious Diseases, Parnaíba Delta Federal University (UFDPar), Parnaíba, PI 64202-020, Brazil

[5] Biodiversity and Biotechnology Research Center, Federal University of Delta Do Parnaíba (UFDPar), Parnaíba, PI 64202-020, Brazil

[6] Institute of Chemistry, Federal University of Rio de Janeiro (UFRJ), Rio de Janeiro, RJ 21941-853, Brazil

[7] Laboratory for the Isolation and Transformation of Organic Molecules, Institute of Chemistry, University of Brasília (UnB), Brasília, DF 70910-900, Brazil

[8] Institute of Physics, University of Brasilia (UnB), Brasilia, DF 70910-900, Brazil

[9] Brazilian Agricultural Research Corporation (EMBRAPA), Embrapa Agroenergy, Brasília, DF 70770-901, Brazil

Published online: 08 January 2024

1 Introduction

Metallic nanoparticles (MNPs) are structures with at least one dimension smaller than 100 nm and are among the most widely used nanomaterials in the industrial and service sectors [1, 2]. Among MNPs, silver nanoparticles (AgNPs) have stood out given their size, shape, and high surface area to volume ratio characteristics that make them ideal for use in various areas, such as antimicrobial and antiparasitic agents, catalytic agents, environmental remediation agents, active cosmetic ingredient, among others [3–6]. Several physical and chemical approaches have been performed for the synthesis of AgNPs; however, they are gradually being substituted due to their inherent shortcomings, which encompass the release of compounds detrimental to both human health and the environment. Furthermore, these approaches are expensive and demand higher reactivity and labor intensity [7–9].

To deal with such limitations and drawbacks, the need for a sustainability-efficient synthesis strategy has led to the establishment of green synthesis. Three initial steps are involved: the choice of solvent medium, the choice of silver ion (Ag^+) reducing agents, and the choice of biocompatible materials for stabilizing AgNPs [10, 11]. In general, biological systems or part of them synthesize AgNPs on a large scale without potentially hazardous reagents, high energy expenditure, and even in a shorter time. In this scenario, plants stand out since their different parts can be exploited and mainly because they have in their phytochemical composition a rich source of plant biomolecules (phenolic compounds, proteins, polysaccharides) that may be responsible for the processes of reduction, capping and stabilization of the surface of the AgNPs formed, reducing the risk of toxicity, and promoting potential improvements in the bioactivities of nanostructures [12–14].

The Amazon is a biome comprising an extensive territorial area, and its biodiversity emerges as a source of valuable resources with a high potential for developing novel technologies applied to science and technology. This aspect configures good perspectives for nanotechnology since, in this region, several plant species can be explored sustainably, for example, in the green synthesis of AgNPs. Guarana (*Paullinia cupana* Kunth) belongs to the Sapindaceae family and is a native Brazilian species with considerable economic and social importance [15], where the seed is generally the commercially exploited part of the plant due to its high phytochemical content, revealing in its composition the presence of various functional biomolecules such as methylxanthines and tannins through extraction using different solvents [16] and also polyphenols such as catechins and procyanidins, as well as the puric alkaloid caffeine, which have been identified in extracts of *Paullinia cupana* seeds from different guarana producing regions of Brazil [17, 18]. There is a report describing the presence of the alkaloids theobromine, theophylline and caffeine in the leaves, stems, inflorescences and pericarps of *Paullinia cupana*, mainly in young/immature tissues and decreasing as the plant matures [19]. Besides the performance of guarana as a source of functional food having stimulant, diuretic, and antioxidants effects [20], its biological actions involve antimicrobial [21], anti-inflammatory [22, 23] and anticancer activities [24].

Biological synthesis routes of AgNPs can be employed to reduce or eliminate the generation of hazardous substances throughout the process, thus improving the sustainability and applicability of the produced nanomaterials [25]. Several techniques exploiting equipment and energy sources have been applied and, combined with natural precursors (e.g., plant extracts), gather features such as low cost, short reaction times and easy reproducibility. However, when analyzing the different parameters involved in the preparation of AgNPs, there are still gaps regarding the combinations between them that result in good characteristics related to yield, shape, size, and stability of nanostructures, since each plant has overly complex phytochemical compositions and the mechanisms associated with the success of phytosynthesis are not yet fully understood [26]. Thus, the present study aimed to synthesize and characterize AgNPs using an aqueous extract of guarana leaves by different routes: autoclave, LED light, microwave, sunlight, ultrasound, and water bath. Furthermore, the antibacterial, leishmanicidal, and cytotoxicity activities of AgNPs were investigated.

2 Material and methods

2.1 Preparation of the aqueous extract of *Paullinia cupana* leaves

Guarana leaves were collected from a private property in the city of Maues, Amazonas State, Brazil (03°22′07″ S and 57°41′27″ O) according to the recommendations of the Genetic Heritage Management Council (CGEN) with authorization number A5C4D66. About 1.0 g of the plant material was weighed, washed with neutral detergent, and with distilled water, and finally the leaves were dried under room temperature to constant weight and cut into small fragments of 5 mm^2. The aqueous extract was prepared by boiling on a hotplate using boiling ultrapure water for 3 min in a ratio 1:10 (w/v) making the concentration of 100 mg/mL, and at the end, the resulting extract was filtered with the aid of qualitative filter paper (Whatman n°1) and used immediately after its preparation.

2.2 Synthesis of AgNPs

AgNPs were synthesized in all routes using an aqueous solution of silver nitrate ($AgNO_3$) (Sigma Aldrich, Brazil) at 2 mM (340 µg/mL) and plant aqueous extract concentration set at 2 mg/mL. The suspensions were transferred to test tubes covered with aluminum foil and incubation lasted 180 min in a water bath (AgNPs-WB) and ultrasonic bath (AgNPs-U) (40 kHz; 132 W) at 70 °C; under sunlight (AgNPs-S) with temperature between 24 and 29 °C and under UV light in a LED light emitting equipment (AgNPs-LED) (660 nm; 55W/m^2) under room temperature. The synthesis of AgNPs was also investigated using heating and pressing in an autoclave (AgNPs-A) for one complete cycle (90 min) at 121 °C and with irradiation by microwave heating (AgNPs-M) (1150 W; 2450 MHz) for 1.5 min.

2.3 Phytochemical profiling of *Paullinia cupana* aqueous extract by UHPLC-HRMS/MS

The aqueous extract of guarana leaf was diluted to a concentration of 2 mg/mL in ultrapure water, centrifuged at 13.200 rpm for 10 min and 1 µL was injected into an ultra-high performance liquid chromatography (UHPLC, Nexera X2, Shimadzu Corporation, Japan) consisting of quaternary gradient pump, auto-vacuum degasser, thermostathed column over set at 40 °C. Separations were carried out using an Acquity UPLC HSS-T3 column oven (150 × 2.1 mm, 1.8 µm, Waters Technologies, Milford, MA, USA) and the detection was performed using an ESI-qTOF-HRMS high-resolution mass spectrometer (maXis 4G, Bruker Daltonics, Germany).

Chromatographic separations were performed using the eluents: A (0.1% formic acid in water (v/v)) B (0.1% formic acid in acetonitrile (v/v)) under the following gradient curve: 0% B isocratic for 0.0–1.0 min, 0–25% B for 1.0–9.0 min, 25–50% B for 9.0–14.0 min, 50–100% B for 14.0–17.0 min, 100% B isocratic for 17.0–20.0 min and 0% B for 20.0–25.0 min returning to the initial condition for equilibration. All analyses were performed using a flow rate of 0.4 mL/min. The high-resolution mass spectrometry analyses were achieved using the following instrument settings: positive mode with the source of electrospray operating at 3.6 kV (ESI(+)-MS) and negative mode with the source of electrospray operating at 3.8 kV (ESI(-)-MS). Nitrogen was used as nebulization (4.0 Bar), desolvation gas (9.0 L/min, 200 °C), and collision gas. The auto MS/MS acquisition settings were configured as previously reported by [27].

The UHPLC-HRMS/MS system was operated using the Compass 1.7 package (Bruker Daltonics, Germany), consisting of oTofControl 3.4 and HyStar 3.2 software and the raw data were processed using DataAnalysis 4.2 software (Bruker Daltonics, Germany). The first-order spectra (MS) were evaluated using the SmartFormula tools that predict the elemental formula of the detected ions and Compound Crowler that makes the identification of metabolites in databases (METLIN, KEGG), while the second-order spectra (MS/MS) were evaluated using the MetFrag [28] tool where the candidate molecules are fragmented, and their mass/charge values (*m/z*) are compared with such values obtained in the spectra of the analyzed samples.

2.4 UV/Vis spectrophotometric analysis

The kinetic effects on the formation of AgNPs were monitored by means of measurements in a UV/Vis spectrophotometer (UV1800PC, Phenix) at the wavelength of 450 nm every 30 min for AgNPs-LED, AgNPs-S, AgNPs-U, and AgNPs-WB, every 15 s for AgNPs-M and only at the beginning and end of the incubation of AgNPs-A due to the specifications of these routes. At the end of each reaction, an absorbance curve was obtained for each sample with measurements in the range between 350 and 550 nm to indicate the peak of maximum intensity that is the result of the surface plasmon resonance (SPR) phenomenon of AgNPs.

2.5 Dynamic light scattering (DLS) and electrophoretic mobility (Zeta potential) analysis

The HD, the PdI, and ZP of the AgNPs synthesized by the different routes were measured by DLS and electrophoretic mobility, in a Zetasizer Nano ZS equipment (Malvern Instruments, UK) configured to perform the readings at a temperature of 25 °C, at an angle of 90°, with a helium–neon laser of 633 nm and after stabilization of 120 s. The samples were diluted in a 1:10 (v/v) ratio in ultrapure water and placed in polystyrene cuvettes that were inserted into the equipment that performed the measurements in manual mode with 10 readings in triplicate. To evaluate the effect of storage, aliquots of each AgNPs suspension were previously stored at room temperature (22 °C) and in a refrigerator (4 °C) and the measurements were repeated the next day of the initial synthesis and after 180 days (6 months). The results were represented by the mean ± standard deviation of the mean, processed by ZetaSizer 7.13 software from the same equipment manufacturer.

2.6 Analysis by Fourier transform infrared spectroscopy (FTIR)

FTIR spectroscopy was used to identify the possible functional groups related to the biomolecules present in the aqueous extract of *Paullinia cupana*, as well the groups existing on the surface of the AgNPs. The spectra in the infrared region were acquired with the use of a spectrophotometer in the attenuated reflectance mode—ATR (Vertex 70, Bruker,

USA) with the samples in liquid state. For the analysis, 2 µL of each sample (without previous dilution) were deposited on a diamond crystal and measurements were performed in the region between 4000 and 500 cm^{-1}, with a resolution of 4 cm^{-1} after 96 scans.

2.7 Transmission electron microscopy (TEM)

For all AgNPs synthesized, a volume of 10 µL of undiluted samples (340 µg/mL) was deposited on copper grids covered with Formvar® film and after 1 min the excess of the drop was removed using the filter. The samples were then left in the dark for 24 h for complete drying. Analyses were performed on a Tecnai Spirit G2 transmission electron microscope operating at 120 kV (FEI, USA). The images were obtained randomly by counting the particles of each group of AgNPs with the aid of *Image J* software (National Institute of Health, USA).

2.8 Antibacterial tests

The minimum inhibitory concentration (MIC) assay was performed according to [29] to evaluate the potential antibacterial activity against the Gram-positive bacteria *Staphylococcus aureus* (ATCC 6538) and the Gram-negative bacteria *Escherichia coli* (ATCC 25922) and *Pseudomonas aeruginosa* (ATCC 9027). Initially, the microorganisms were grown on Mueller–Hinton agar at 35 °C for 24 h under aerobic conditions and subsequently, the isolated colonies were suspended in 0.85% isotonic sodium chloride saline with an optical density of 0.5 on the McFarland scale ($1–2 \times 10^8$ CFU/mL). Bacterial suspensions at a concentration of 5×10^5 CFU/mL were inoculated into 96-well microplates and exposed to AgNPs synthesized via the different green synthesis routes and the aqueous $AgNO_3$ solution (0.42 to 54 µg/mL), as well as the aqueous extract of guarana leaves (3.9 to 500 µg/mL). The plates were incubated for 24 h at 37 °C under aerobic conditions and the MIC was defined as the lowest concentration of the tested samples that inhibited visually observed bacterial growth.

2.9 Antipromastigote assay in *Leishmania amazonensis*

Parasites of the species *Leishmania amazonensis* (IFLA/BR/67/PH8) were maintained in vitro in their promastigote form in Schneider medium supplemented with 10% fetal bovine serum (FBS) and 1% solution of penicillin (100 U/mL) and streptomycin (100 µg/mL), pH 7 and incubated at 26 °C in a Biochemical Oxygen Demand (BOD) incubator, according to the methodology of [30]. The assay was performed with promastigote forms in logarithmic growth phase cultured in 96-well plates (1×10^6 parasites/well) in 100 µL of supplemented Schneider medium, containing serial concentrations of AgNPs synthesized by different routes (3.12 to 200 µg/mL), aqueous plant extract, $AgNO_3$ and positive control miltefosine (1.56 to 100 µg/mL). The microplates were incubated in BOD at 26 °C for 72 h and after the treatment period 10 µL of MTT (5 mg/mL) was applied to each well and the plates were incubated again for another 4 h. At the end of the process, 50 µL of 10% sodium dodecyl sulfate (SDS) solution (w/v in distilled water) was added to the wells for the solubilization of formazan crystals. The reading was performed in a microplate spectrophotometer (Biosystems ELx800, Curitiba, Brazil) at 540 nm. The negative control was performed with a supplemented Schneider medium containing 0.2% DMSO, considered as 100% viability of leishmania.

2.10 Determination of cytotoxicity in infected macrophages and calculation of the selectivity index (SI)

Cytotoxicity was assessed in 96-well microplates by MTT colorimetric assay. The RAW 264.7 murine macrophage cell line was cultured in DMEM medium supplemented with 10% fetal bovine serum (FBS) and 1% penicillin (100 U/mL) and streptomycin (100 µg/mL) solution, pH 7, at 37 °C, 5% CO_2 with 80% humidity [31]. A concentration of 1×10^5 RAW 264.7 macrophages per well was placed in 100 µL of supplemented DMEM medium, and after 4 h of incubation at 37 °C and 5% CO_2 for cell adhesion, the wells were washed with sterile PBS. Soon after, in triplicate wells, 100 µL of supplemented DMEM medium containing different concentrations of AgNPs and $AgNO_3$ (3.12 µg/mL to 200 µg/mL), aqueous plant extract (1.56 µg/mL to 100 µg/mL), positive control (miltefosine 6.25 to 400 µg/mL) were added and incubated for a period of 72 h. After incubation, 10 µL of MTT (5 mg/mL) was applied to the wells, and the microplates were incubated again for a further 4 h, then the supernatant was removed and 100 µL of DMSO was added to all wells. After 30 min of stirring, the reading was performed at 540 nm on a plate reader (Biosystems ELx800, Curitiba, Brazil). Supplemented DMEM medium containing 0.5% DMSO was used as negative control and considered 100% macrophage viability.

The SI of each treatment was calculated by dividing the cytotoxicity concentration observed for macrophages (CC_{50}) by half of the maximum inhibition concentration measured for the leishmania species (IC_{50}).

2.11 Statistical analysis

Quantitative data of DLS characterization and Zeta potential of AgNPs, as well as the mean values of dry diameter determination of AgNPs obtained by TEM, are presented

as mean ± standard deviation (SD) of the mean. Possible differences between groups were determined by analysis of variance (ANOVA) followed by Tukey's test with significance level at $p < 0.05$. Graphs and/or histograms were plotted using GraphPrism 8 (GraphPad Software, USA) and OriginPro 8.5 (OriginLab Corporation, USA) software.

3 Results and discussion

3.1 Chemical characterization of *Paullinia cupana* aqueous extract

The chemical profile of the aqueous extract of *Paullinia cupana* leaves used in the synthesis of AgNPs was investigated by UHPLC-HRMS/MS to identify the biomolecules that, among other properties, can act as reduction agents of silver ions (Ag^+) to colloidal silver (Ag^0) and stabilization/coating of the surface of nanostructures, as extensively reported in previous research [32, 33].

Evaluating the Base Peak Chromatogram (BPC) for the compounds 3, 4, and 7 $[M+H]^+$ they showed low retention times ($t_R = 1.000$ min, 1.084 min, and 1.562 min, respectively), an indication of high polar compounds and their precursor ions were highlighted with *m/z* at 176.0915, 148.0973, and 130.0862, being putatively identified as calistegin B2, fagomine, and pipecolic acid, respectively. On the other hand, compound 9 was eluted at $t_R = 8.332$ min and its precursor ion was observed as an intense signal at *m/z* 181.0722 $[M+H]^+$ and it was putatively characterized as theobromine (Fig. 1a; Supplementary Table S1).

When evaluated in negative mode the BPC (Fig. 1b) revealed a precursor ion at *m/z* 191.0566 $[M+H]^-$ for the high polar compound 7 ($t_R = 1.243$ min) and it was putatively attributed to the quinic acid. At the end of BPC are highlighted three well-defined peaks ($t_R = 14.262$ min, 14.933 min, and 15.752 min), where their precursor ions were defined as *m/z* 449.1110, 447.0950 and 431.0997 $[M+H]^-$ revealed the presence of the compound 11 astilbin, compound 12 quercitrin, and compound 14 afzelin, respectively (Supplementary Table S1). Recently, isoquercitrin was found as the main compound in the plant *Sambucus ebulus* and was considered by the authors the main metabolite related the biosynthesis of AgNPs with bioactive properties [34].

Different analytical responses were obtained when the UHPLC-HRMS/MS system was used in distinct ionization mode. Four compounds were identified when positive ionization was used and the other four by the negative mode. To the best of our knowledge, this appears to be the first scientific report involving the characterization of aqueous extracts of *Paullinia cupana* leaves, which may provide support for further research dealing with the main compounds present in this kind of plant phytopreparation.

Among the mechanisms proposed for the reduction of Ag^+ ions to Ag^0 there is the influence of free electrons from

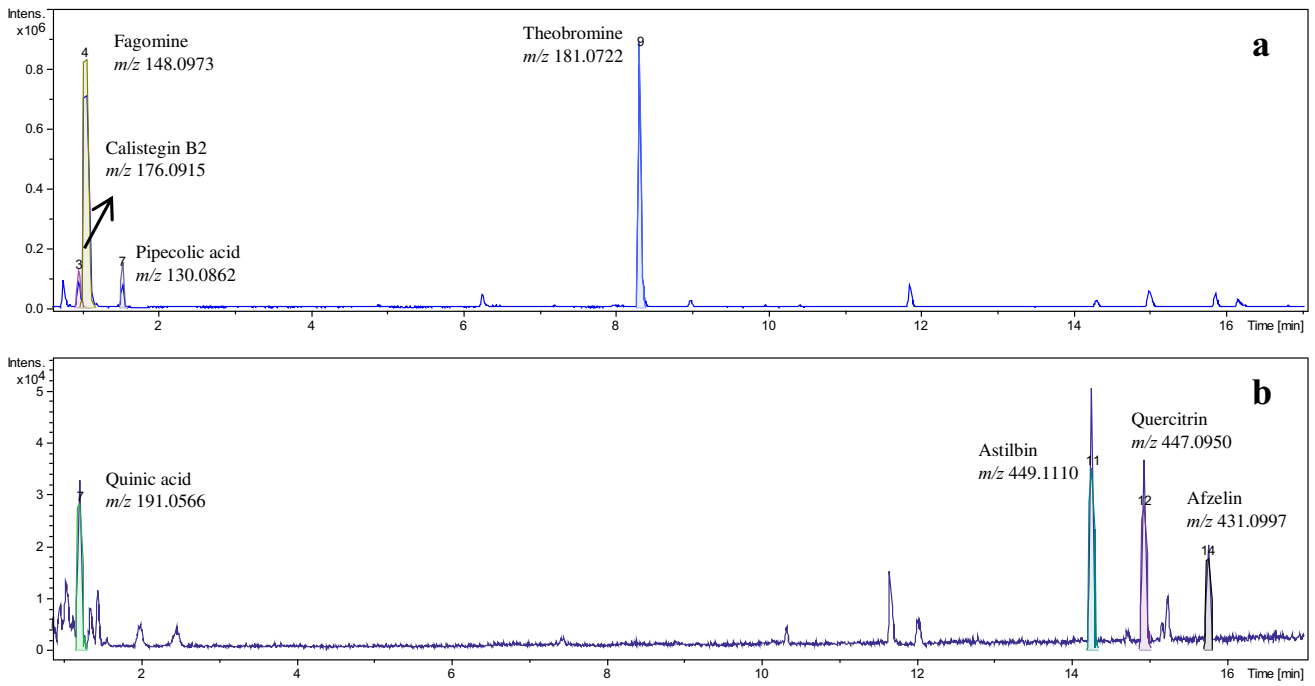

Fig. 1 Chromatograms obtained by UHPLC-HRMS/MS of the aqueous extract of *Paullinia cupana* leaves collected in the dry period. **a** Positive ionization mode; **b** Negative ionization mode

functional groups (hydroxyls, carboxyls, carbonyls, amines) present in biomolecules, mainly phenolic acids, alkaloids and flavonoids that make up the aqueous extract of *Paullinia cupana* leaves (Supplementary Fig. S1) and that, through the process of chelation with the metal, organize themselves into stable complexes, resulting in the formation of AgNPs [35, 36], as described in some research that explored caffeine, theophylline, quercetin and naringenin as the main metabolites responsible for the bioreduction and stabilization of silver nanostructures [37–39]. In general, through the low dissociation energy of hydroxyl groups (-OH) during the tautomeric transformation of compounds from the enol form to the keto form, there is the release of cationic hydrogen atoms that are bound to silver for subsequent biological reduction [40–42].

3.2 Visual aspect and UV/Vis spectral analysis

Color changes of colloidal suspensions are among the most widely used available approaches to monitor the formation of AgNPs. This visual property has been related to the SPR effect, which, among other factors, can depend on the potentially formed nanostructures optical, structural, and morphological features [43]. With this, in the present study, it is possible to observe a similar coloration of all the reaction mixtures after the synthesis time for each equipment and/or energy source used, tending to a yellowish hue (Supplementary Fig. S2).

Monitoring the absorbance at a wavelength of 450 nm carried out throughout the synthesis reactions based on the specifications of each route showed that, based on the absorbance intensity obtained, all the routes employed resulted in the formation of AgNPs regardless of the intrinsic conditions in each condition adopted (Fig. 2). Temperature is an essential factor during the bioreduction process, as it can control the kinetics of the reaction and the physicochemical characteristics of the nanostructures synthesized by increasing the electron transport of the biomolecules present in the plant extracts that meet Ag^+ ions, efficiently promoting their conversion into Ag^0 [44, 45]. Thus, the time and type of route used could significantly influence the synthesis of AgNPs in the present study.

The routes that used an autoclave and sunlight reached maximum absorption right at the start of monitoring in the UV/Vis spectrum due to their intense coloration. Therefore, these aliquots were diluted to continue their spectral characterizations and, as can be seen in Fig. 2, the AgNPs-S curve showed an almost stabilization phase, while the AgNPs-A curve showed the formation of nanostructures even with a shorter reaction time. The method that uses heating and pressure in an autoclave can favor the initial nucleation stage of the nanoparticles by controlling their size and shape, while synthesis under direct solar irradiation is favored by the photons of light that accelerate the bioreduction reactions by acting as catalysts that allow the process to take place in less time [46–48].

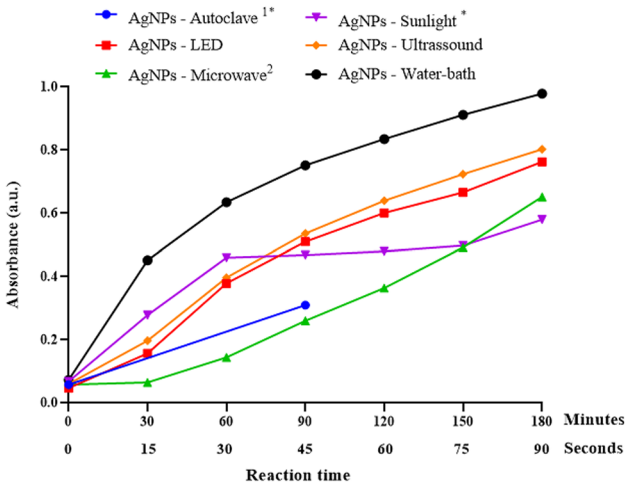

Fig. 2 Kinetic curves monitoring the formation of AgNPs obtained by spectrophotometry at 450 nm during biosynthesis using the aqueous extract of *Paullinia cupana* leaves varying the equipment and/or energy source. [1]Absorbance was measured only at the beginning and end of the reaction; [2]Absorbance was measured every 15 s for a time of 1.5 min. *Samples were diluted 1:10 (v/v) in ultrapure water

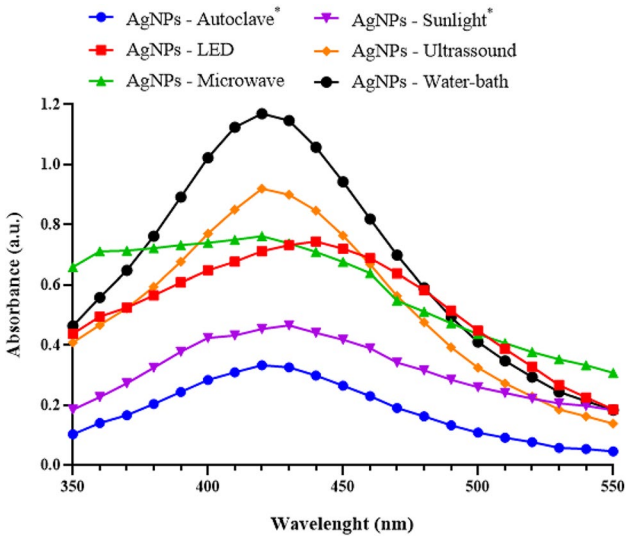

Fig. 3 Absorbance curves of AgNPs obtained by spectrophotometry in the range 350 to 550 nm after the biosynthesis time using the aqueous extract of *Paullinia cupana* leaves varying the equipment and/or energy source. *Samples were diluted 1:10 (v/v) in ultrapure water

The absorption curves of the AgNPs samples (Fig. 3) reveal that the maximum peak is 420 nm for AgNPs-A, AgNPs-M, AgNPs-U, and AgNPs-WB, with small shifts to longer wavelength regions, maximum absorption bands at 430 nm for AgNPs-S and 440 nm for AgNPs-LED, typical the silver metallic nanostructures. These subtle changes in

the UV/Vis spectra of AgNPs may correlate with the SPR phenomenon that may also be responsible for the color change of the reaction mixtures and vary due to factors such as size, shape, concentration of biomolecules used in the synthesis, reaction temperature, among others [49, 50].

3.3 Evaluation of colloidal stability by DLS and surface Zeta potential

In the present study, DLS and Zeta potential measurements occurred right after the syntheses, the next day, and 180 days after the initial synthesis with the AgNPs stored under room temperature (~22° C) and in the refrigerator (~4° C). The results are described in Table 1.

According to the HD data, the size distribution range of AgNPs on the day of synthesis by each proposed route was between 64.7 and 97.55 nm. Over 180 days, such measurements were significantly lower ($p < 0.05$) when the values of AgNPs-LED and AgNP-U were compared to their initial sizes, regardless of storage, but increased significantly ($p < 0.05$) when the values of AgNPs-S and AgNPs-WB were evaluated after storage in a refrigerator. When using *Aloe vera* leaf extract, the authors synthesized AgNPs with a diameter of 88.78 nm [51], like that described in the present study for AgNPs-S. In turn, the extract from the leaves of *Barleria buxifolia* mediated the synthesis of AgNPs with a diameter of 80 nm after exposure to ultrasound irradiation [52], this size being higher than the sizes observed 180 days after the synthesis of AgNPs-U.

The PdI, a parameter that provides information on the homogeneity of distribution of particles in suspension, was considered moderate to high for all synthesized samples (0.2–0.5) and may indicate the formation of agglomerates related to modifications on the surfaces of nanostructures [53]. After 180 days of synthesis, the PdI of AgNPs-M, AgNPs-U, and AgNPs-WB decreased significantly ($p < 0.05$) compared to those newly synthesized regardless of the storage environment, demonstrating that over time it is possible to modulate the characteristics related to the homogeneity of the synthesized AgNPs. When using LED light at different wavelengths in the green synthesis of AgNPs from *Bougainvillea glabra*, a polydispersity range between 0.209 and 0.504 similar was observed with the data obtained for AgNPs-LED during colloidal stability analyses [54]. On the other hand, our results for AgNPs-M are more satisfactory than those recently reported in a study that obtained AgNPs via Sycamore at different pHs with PdI between 0.25 and 0.5 [55].

All newly synthesized AgNPs showed high values of Zeta potential, highlighting AgNPs-M and AgNPs-WB with surface charges of − 38.1 mV and − 36 mV, respectively, agreeing with previous research where the water bath method used in biosynthesis allowed AgNPs to be obtained with a surface charge of around − 36.7 mV [56]. These measurements represent the electrical interactions between the surface of the particles with the liquid

Table 1 Hydrodynamic diameter (HD), polydispersity index (PdI) and surface Zeta potential (ZP) of AgNPs biosynthesized from aqueous extracts of *Paullinia cupana* leaves employing different equipment and/or energy source on the day of synthesis (D0), after 1 day (D1) and after 180 days (D180) from the initial synthesis with storage at room temperature (RT) – 22 °C or in refrigerator (REF) – 4 °C

Time/Storage	HD (nm)	PdI	ZP (mV)
AgNPs-A			
D0	76.73 ± 1.4	0.284 ± 0.01	− 33 ± 1.6
D1 – RT	77.33 ± 0.7	0.303 ± 0.04	− 30.3 ± 4.9
D1 – REF	72.36 ± 2.5	0.272 ± 0.02	− 32 ± 0.8
D180 – RT	77.3 ± 1.5	0.288 ± 0.02	− 30.9 ± 0.7
D180 – REF	79.18 ± 4.7	0.302 ± 0.04	− 31.7 ± 0.7
AgNPs-LED			
D0	87.76 ± 4.6	0.428 ± 0.01	− 34.4 ± 1.6
D1 – RT	62.56 ± 1.9 ϕ	0.341 ± 0.05	− 36.2 ± 2.3
D1 – REF	72.42 ± 3.1 ϕ	0.396 ± 0.03	− 28.7 ± 1.9 ϕ
D180 – RT	55.85 ± 1.8 ϕ	0.518 ± 0.08	− 37.2 ± 0.9
D180 – REF	53.1 ± 2.1 ϕ	0.472 ± 0.06	− 34.9 ± 1.6
AgNPs-M			
D0	64.7 ± 9.1	0.894 ± 0.18	− 38.1 ± 0.3
D1 – RT	38.43 ± 5.3 *	0.874 ± 0.22	− 31.6 ± 4.0 *
D1 – REF	37.53 ± 5.4 *	0.874 ± 0.22	− 31.2 ± 2.7 *
D180 – RT	77.21 ± 14.2	0.373 ± 0.08 *	− 32.6 ± 0.7
D180 – REF	71.08 ± 7.5	0.260 ± 0.02 *	− 35.4 ± 0.7
AgNPs-S			
D0	75.86 ± 1.3	0.395 ± 0.06	− 33 ± 2.9
D1 – RT	74.25 ± 0.1	0.333 ± 0.01	− 33.8 ± 1.8
D1 – REF	68.5 ± 1.0	0.419 ± 0.02	− 37.5 ± 0.4
D180 – RT	77.56 ± 2.7	0.427 ± 0.04	− 33.5 ± 0.4
D180 – REF	92.23 ± 8.4 β	0.389 ± 0.10	− 32 ± 2.2
AgNPs-U			
D0	97.55 ± 2.2	0.476 ± 0.01	− 32.9 ± 1.3
D1 – RT	72.14 ± 2.7°	0.418 ± 0.01	− 37.2 ± 1.2°
D1 – REF	72.53 ± 1.2°	0.404 ± 0.07	− 36 ± 0.7°
D180 – RT	76.17 ± 0.6°	0.278 ± 0.01°	− 34.9 ± 0.4
D180 – REF	72.3 ± 1.1°	0.351 ± 0.03°	− 33.5 ± 1.3
AgNPs-WB			
D0	74.57 ± 4.8	0.462 ± 0.06	− 36 ± 1.1
D1 – RT	66.46 ± 1.6 ˣ	0.403 ± 0.01	− 35.5 ± 1.2
D1 – REF	68.55 ± 1.6	0.456 ± 0.03	− 32.3 ± 3.1
D180 – RT	68.94 ± 0.1	0.319 ± 0.04 ˣ	− 35.6 ± 0.9
D180 – REF	85.93 ± 2.4 ˣ	0.365 ± 0.06	− 34.5 ± 1.3

Values are represented as mean ± standard deviation of the mean of measurements in triplicate. Statistical analysis: one-way ANOVA test ($p < 0.05$), followed by Tukey's test. Superscript symbols indicate significant differences within each parameter separately for each AgNPs group compared to the day 0 (D0) measurement, where ϕ = AgNPs-LED; * = AgNPs-M; β = AgNPs-S; ° = AgNPs-U; ˣ = AgNPs-WB.

medium to which they are dispersed and are related to electrostatic attraction phenomena at this interface [57]. It is important to highlight that, even after evaluation for 6 months in different storage conditions, no Zeta potential measurement had significant change ($p < 0.05$) when compared to the measurement of newly synthesized AgNPs, which may mean the maintenance of colloidal stability of nanostructures in aqueous suspension.

With a view to large-scale production and increasingly robust optimizations to achieve better results, it is of fundamental importance to monitor the colloidal stability of AgNPs synthesized from different routes since each method has intrinsic characteristics that can influence colloidal properties over time and considering the distinct phytochemical composition of plants that can behave differently in the process of stabilizing the surface of the particles.

3.4 FTIR analysis

FTIR spectroscopy was used to characterize and identify the chemical composition of the AgNPs surface. This analysis contributed to determine which are the likely molecules that acted as capping and reducing agents of AgNPs. The FTIR spectrum of guarana aqueous extract is showed in Fig. 4a and as indicated presents bands at 3346, 2938, 2850, 1700, 1620, 1398, 1078 and 660 cm^{-1} which are associated with vibrational modes of the hydroxyls, carboxyls, carbonyls, and amines, among others functional groups, from the classes of phytochemicals related to the guarana plant material involved in the AgNPs formation process.

Due to the compositional complexity of the guarana extract, there may be overlapping of the absorption bands of the different functional groups, which makes it difficult to correctly assign these bands in the AgNPs spectra

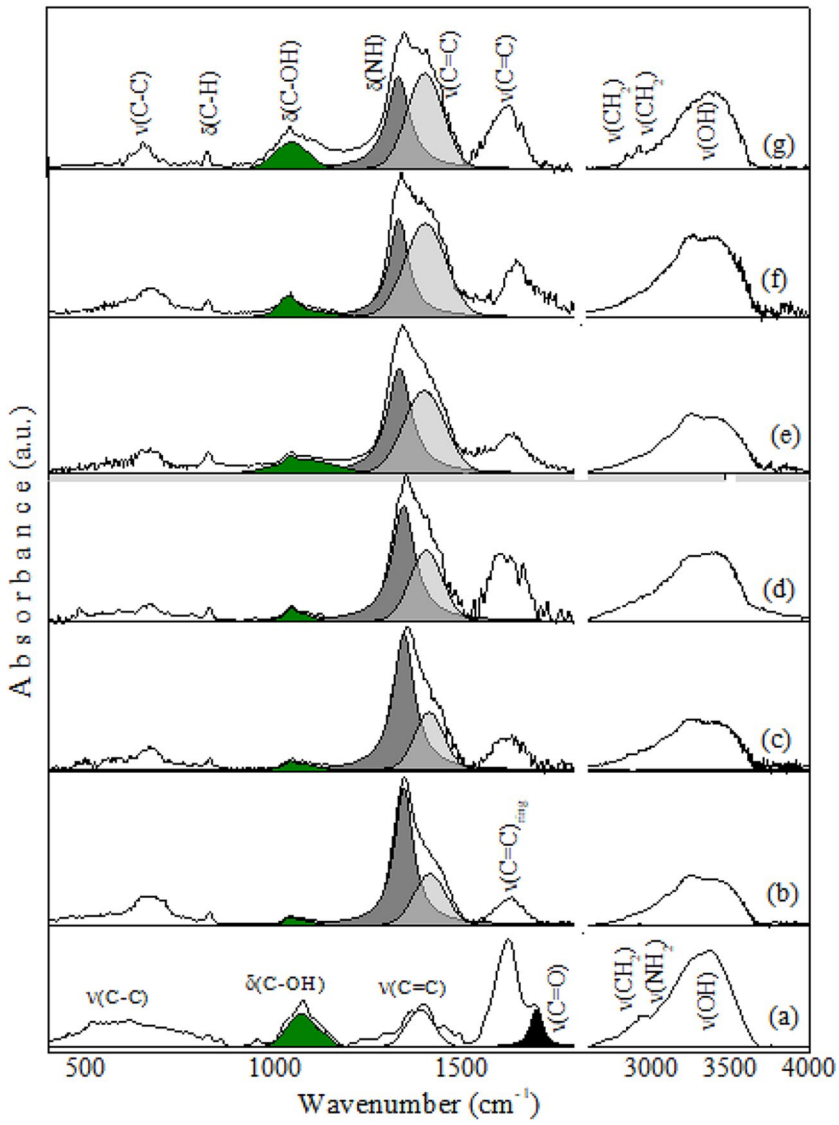

Fig. 4 FTIR spectra of extract of (**a**) *Paullinia cupana* leaves and AgNPs synthesized with different synthesis routes: (**b**) AgNPs-U, (**c**) AgNPs-WB, (**d**) AgNPs-A, (**e**) AgNPs-M, (**f**) AgNPs-S, and (**g**) AgNPs-LED

synthesized with different synthesis routes (Fig. 4b–g). For example, the bands ranging from 3200 to 3600 cm^{-1} are related to the stretching vibrations of the O–H (due to hydroxyl groups) and N–H (due to amides groups) of the phytochemicals compounds, while the bands at 2924 and 2850 cm^{-1} (AgNPs-LED) can be assigned to antisymmetric and symmetric stretch modes of CH_2 of alkanes [58] and were also found in the spectrum referring to the *Paullinia cupana* extract as 2938 cm^{-1}, corroborating with previous studies that found who found a peak around this region in spectra that analyzed the extract of the guarana seed residue [59]. The band around 1700 cm^{-1} in the extract spectrum is related to C = O stretching vibration of the carbonyl group; however, the stretching vibrations of amides (-$CONH_2$) also appear in this range. In addition, in relation to AgNPs, the band around 1620 cm^{-1} can be correlated to the stretching of aromatic C = C bond of phytochemicals compounds and may also correspond to the N–H bending of aromatic amines present in the guarana biomolecules, as previously reported in FTIR spectra analysis of *Paullinia cupana* seed extract [60]. In turn, the bands around 1345, 1040, and 660 cm^{-1} in the AgNPs spectrum are characteristic of the C = C ring stretching, C–OH bending, and C–C ring stretching vibrations, respectively [61].

In general, the FTIR spectra of AgNPs synthesized with different routes show spectral feature like those of guarana extract, indicating the presence of phytochemicals compounds at the nanoparticles surfaces. However, it is important to note in the spectra of the AgNPs samples, the disappearance of the peak at 1700 cm^{-1}, the appearance of a peak at near 1330 cm^{-1} (marked in dark gray) and the increase in the intensity of the bands around 1065 and 1395 cm^{-1} (marked in green and light gray, respectively). Indeed, it was observed that the integrated intensity of these bands is twice as high in the AgNPs samples synthesized at lower temperatures (AgNPs-S and AgNPs-LED when compared to those synthesized at temperatures greater than 70 °C (AgNPs U, AgNPs-WB, AgNPs-A, and probably AgNPs-M), considering that most of the phenolic compounds are heat-sensitive, which leads to a greater degradation of these compounds in the samples synthesized at higher temperatures [62]. Thus, since all the colloidal suspensions were prepared with the same concentration of metallic precursor and aqueous plant extract, the synthesis routes involving different equipment and/or energy sources (implying in greater or lesser energy, and intramolecular forces/interactions), could explain this behavior, as well as the shifts (wavenumber – cm^{-1}, x-axis), widths, shapes, and the relative intensity (absorbance — %, y-axis), of the peak/band observed.

Related to the bio-reduction process, the $AgNO_3$ salt, when dissolved into water, is broken up into two ions (Ag^+ and NO_3^-). Since OH and COOH groups from phytochemical compounds are acidic in nature, they supply H^+ and acquire a negative charge (O^- and COO^-), which form electrostatic linkage with the Ag^+ ions, reducing Ag^+ to Ag^0, that start to aggregate forming clusters which grow further and finally stabilize to form AgNPs [63]. The peak around 1340–1354 cm^{-1} in the AgNPs spectra can be explained by considering that NO_3^- ions can accept H^+ from OH of phenol or from COOH of the acid of the polyphenolic compounds to form HNO_3, which remains in the aqueous phase, giving rise to the mode vibrational δ(NH) [64, 65].

3.5 Morphological TEM analysis

The morphological and two-dimensional characteristics can be affected by the parameters investigated when obtaining the AgNPs, including the biological synthesis routes. Figure 5 shows that the morphology of the AgNPs revealed a predominantly almost spherical shape, even if the particles have irregular edges with at least one other less frequent geometric shape, among which are rod, ellipsoidal and triangular shapes, demonstrating that the *Paullinia cupana* leaf extract is efficient in forming nanostructures with different morphologies and no signs of aggregation. Another prominent factor is the shaded coverage around the surface of AgNPs which refers to the immobilization and coating made by biomolecules from the aqueous plant extract, a common fact to be observed in biogenic nanostructures and which is responsible for their stabilization [66, 67].

Based on Mie theory, the presence of only one maximum absorption band in the UV/Vis spectra is characteristic of spherical nanostructures and by presenting peaks at different wavelengths AgNPs can have distinct shapes and sizes [68, 69]. According to Fig. 5, with the smallest dry diameter, AgNPs-A stood out with 13.08 ± 6.3 nm while the largest sizes were AgNPs-M and AgNPs-U with 47.54 ± 12.32 nm and 61.1 ± 19.1 nm, respectively. In turn, the other samples had similar diameters, being 20.86 ± 11.65 nm (AgNPs-LED), 23.51 ± 15 nm (AgNPs-S) and 29.42 ± 18.8 nm (AgNPs-WB). It is possible to infer that the disparity between the TEM values when compared to the DLS results occurs considering the aqueous solvation layer that covers the surface of the AgNPs and the number of particles counted in each analysis.

3.6 Antibacterial activity

The bacterial susceptibility caused by AgNPs, aqueous plant extract of *Paullinia cupana* leaves, and aqueous $AgNO_3$ solution was evaluated from the determination of the minimum inhibitory concentration (MIC), and the results are presented in Table 2.

The results showed that the inhibitory effects on the *Escherichia coli* were more significant when using AgNPs-LED, AgNPs-M, AgNPs-U, and AgNPs-WB with MIC of

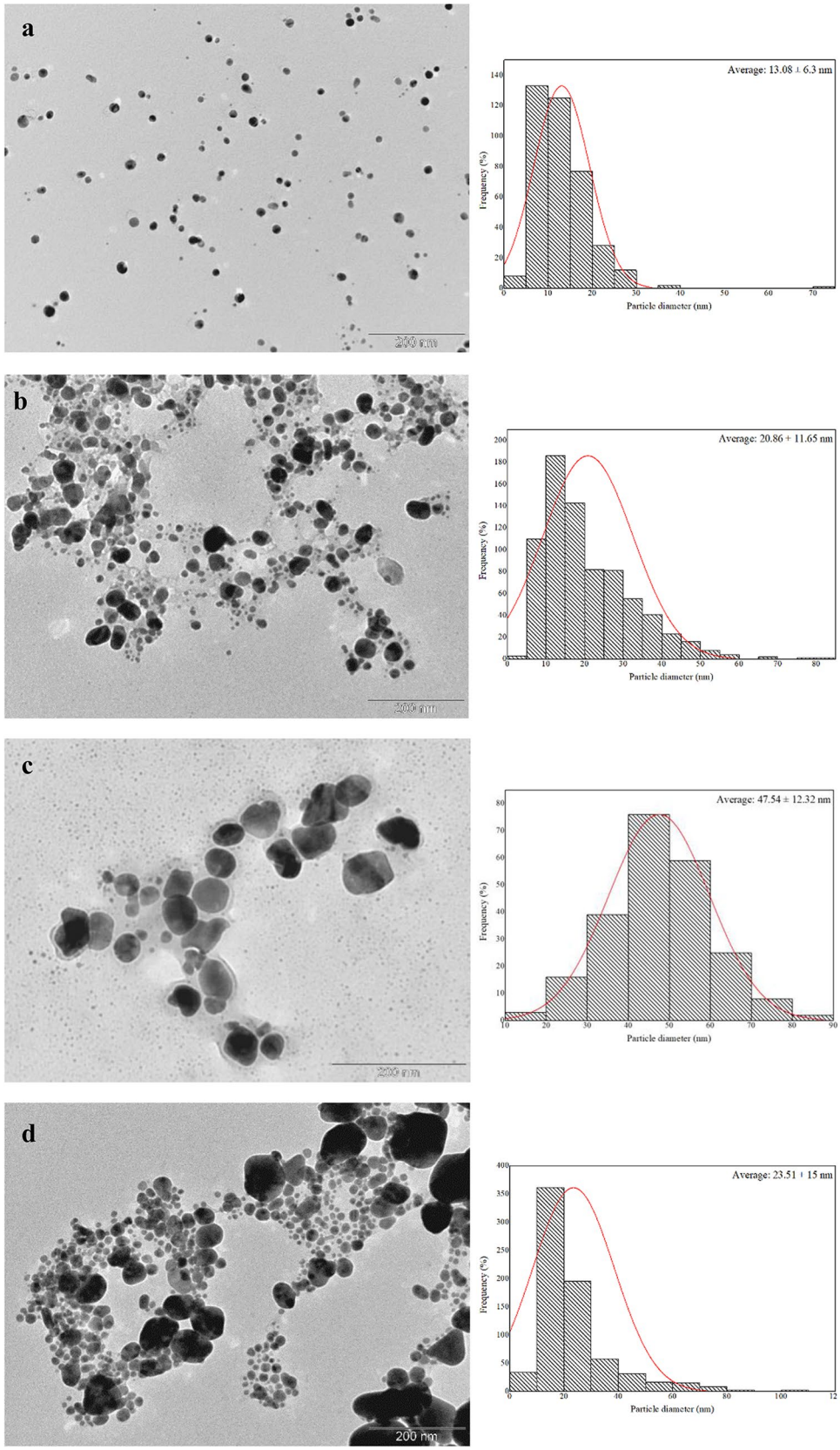

Fig. 5 Micrographs obtained by MET and their respective dry diameter distribution histograms of AgNPs-A (**a**), AgNPs-LED (**b**), AgNPs-M (**c**), AgNPs-S (**d**), AgNPs-U (**e**) and AgNPs-WB (**f**)

Fig. 5 (continued)

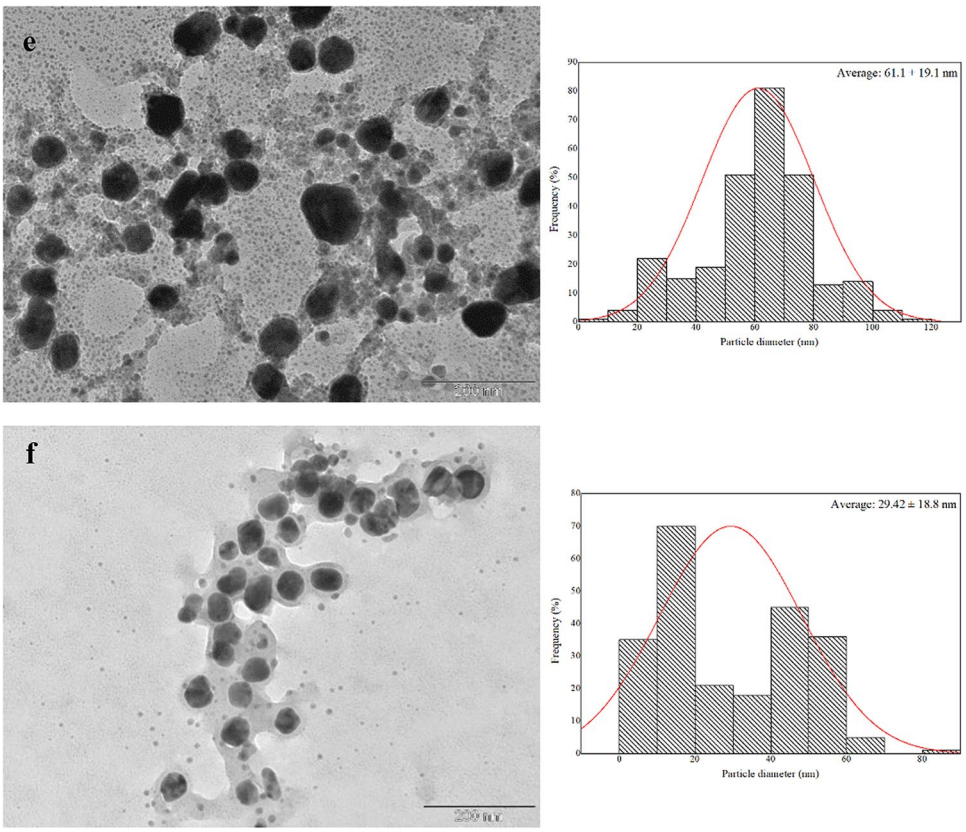

Table 2 Minimum inhibitory concentration (MIC) of AgNPs synthesized from different synthesis routes, leaves aqueous extract of *Paullinia cupana* and silver nitrate solution ($AgNO_3$) against Gram-positive and Gram-negative bacteria after 24 h of treatment

Samples	*Escherichia coli* (ATCC 25922)	*Pseudomonas aeruginosa* (ATCC 9027)	*Staphylococcus aureus* (ATCC 6538)
		MIC (μg/mL)	
AgNPs-A	10.62	2.65	10.62
AgNPs-LED	5.31	5.31	10.62
AgNPs-M	5.31	2.65	5.31
AgNPs-S	21.25	10.62	21.25
AgNPs-U	5.31	2.65	10.62
AgNPs-WB	5.31	2.65	10.62
$AgNO_3$	10.62	2.65	21.25
AE	> 500	> 500	> 500

A autoclave, *LED* LED light, *M* microwave, *S* sunlight, *U* ultrasound, *WB* water bath, *AE* aqueous extract of *Paullinia cupana* leaves

5.31 μg/mL. For the *Pseudomonas aeruginosa*, AgNPs-A, AgNPs-M, AgNPs-U, and AgNPs-WB had greater antibacterial efficacy, presenting MIC of 2.65 μg/mL. When evaluating the MIC against *Staphylococcus aureus*, it is possible to observe that the highest sensitivity came after treatment with AgNPs-M (5.31 μg/mL), since all other suspensions containing the nanostructures had values at least twice as high, being more efficient than AgNPs synthesized from aqueous extracts of other Amazonian plants and reported in our previous study [70]. The aqueous $AgNO_3$ solution was more effective against Gram-negative bacteria (2.65 μg/mL and 10.62 μg/mL) than *Staphylococcus aureus* (21.25 μg/mL) and, in this study, the aqueous extract of *Paullinia cupana* leaves presented MIC above 500 μg/mL, unlike that reported with the extract of the seeds of this plant that had MIC of 250 μg/mL for several bacteria, including *Escherichia coli* and *Staphylococcus aureus* [71].

From these results, it can be inferred that Gram-negative bacteria showed greater susceptibility to most of the biogenic AgNPs tested, and this effect is related to the peptidoglycan layer in their cell wall, which is thinner compared to the layer of Gram-positive bacteria [72, 73]. Other prominent factors that may have contributed to the observed actions regarding the inhibition of bacterial growth caused by AgNPs are the presence of transport proteins (porins) found in the outer membranes of bacteria allowing the entry of metal ions, in addition to the morphological and dimensional characteristics of nanostructures that result in greater surface area and have an influence on antibacterial effects [74, 75].

The surface electric charge of AgNPs can significantly affect their antimicrobial properties by influencing the

electrostatic attraction/repulsion phenomenon. Even if the surface charges of the AgNPs produced in this study are negative, antibacterial activity occur due to interaction with sulfur-containing amino acids, such as cysteine and methionine, causing severe damage that ultimately results in the rupture of the bacterial cell membrane [76–78]. Another highlight is that, at higher concentrations of AgNPs, the effect against bacteria may be due to crowding molecular that causes the cell to suffer osmotic compression, loss of homeostasis, decreased diffusion rates, in addition to reduced biochemical activities, structural changes in the cytoplasm and changes in electrostatic interactions [79–81].

Ultimately, apart from the inherent characteristics of AgNPs that underlie their effectiveness in antibacterial activity, certain biomolecules found in the aqueous extract of *Paullinia cupana* leaves, used as coating agents on the surface of silver nanostructures, may also contribute synergistically to this effect. Pipecolic acid, quercetin, afzelin, and quinic acid were identified as potential contributors to the inhibition of *Staphylococcus aureus* growth [82]. Additionally, astilbin was noted for its antimicrobial effects against *Pseudomonas aeruginosa* and *Staphylococcus aureus* [83].

3.7 Antileishmania activity

The leishmanicidal activity was evaluated on promastigote forms of *Leishmania amazonensis* after 72 h of incubation with AgNPs, aqueous extract of *Paullinia cupana* leaves, aqueous $AgNO_3$ solution, and miltefosine drug (standard drug). The results of the treatments are shown in Table 3.

It is possible to observe that the parasites were more sensitive to the effects of AgNPs-M, AgNPs-U, AgNPs-LED, and AgNPs-WB with IC_{50} values of 5.8 µg/mL, 5.6 µg/mL 7.53 µg/mL and 7.07 µg/mL, respectively. These results indicate that the loss of parasite viability can be achieved at low concentrations of AgNPs and further modulated according to the type of route employed on the synthesis of the nanostructures, similar to previous research where AgNPs were synthesized using water bath from *Fagonia indica* leaf extracts with IC_{50} value of 4.8 µg/mL on *Leishmania tropica* promastigotes and by microwave method where compounds from *Anarcadium occidentale* were used to stabilize AgNPs with action on *Leishmania braziliensis* expressing IC_{50} values between 11.54 µg/mL and 86.61 µg/mL [84, 85].

The degree of growth inhibition revealed that AgNPs-A had an IC_{50} of 24.52 µg/mL, and this value was close to that obtained by the drug miltefosine (IC_{50} value of 17.25 µg/mL), while AgNPs-S had an IC_{50} value of 57.27 µg/mL, which was higher than that obtained after exposure of the organisms to $AgNO_3$ (IC_{50} value of 54.8 µg/mL). Furthermore, although the extract of *Paullinia cupana* leaves did not cause significant effects on the loss of parasite viability in the present study, some extracts of Amazonian plants were previously investigated and showed inhibitory activities against the growth of *Leishmania amazonensis*, for example, *Croton cajucara* (IC_{50} 12.07 µg/mL), *Annona foetida* (IC_{50} 16.2 µg/mL) and *Copaifera reticulata* (IC_{50} 5 µg/mL) [86–88], demonstrating the potential of the Amazon biome to offer leishmanicidal plant metabolites potentially active against neglected diseases.

Table 3 Antipromastigote activity (IC_{50}), cytotoxicity against macrophages (CC_{50}) and SI of AgNPs synthesized from varying synthesis routes, aqueous extract of *Paullinia cupana* leaves and silver nitrate ($AgNO_3$) solution

Samples	IC_{50} (µg/mL)	CC_{50} (µg/mL)	SI
AgNPs-A	24.52	71.48	2.92
AgNPs-LED	7.53	90.4	12
AgNPs-M	5.8	79.26	13.66
AgNPs-S	57.27	164.1	2.86
AgNPs-U	5.6	83.67	14.94
AgNPs-WB	7.07	91.39	12.93
$AgNO_3$	54.8	61.35	1.12
AE	> 100	> 100	> 1
Miltefosine	17.25	241.1	13.97

SI CC50/CI50, *A* autoclave, *LED* LED light, *M* microwave, *S* sunlight, *U* ultrasound, *WB* water bath, *AE* aqueous extract of *Paullinia cupana* leaves

The spherical shape of the AgNPs studied here facilitates their entry into cells through phagocytosis [89]. Once inside, the AgNPs break through the cell membrane and enter the cytoplasm. Here, they undergo oxidation, generating Ag^+ ions, which are considered the main agents responsible for killing the parasite. These ions can interact with thiol groups within the DNA, inhibiting parasite replication and leading to cell cycle arrest in the G0/G1 phase [90]. In addition, Ag^+ ions interact with the parasites respiratory system, producing reactive oxygen species (ROS) and nitric oxide (NO) [91, 92]. Another important factor is that metal ions can inhibit enzymes essential for parasite metabolism by interacting with their thiol (-SH) groups, which leads to cytotoxic processes and cell death by necrosis [93–95].

3.8 Cytotoxicity analysis

To obtain safety and increase their spectrum of use, the AgNPs synthesized in the present study, in addition to the aqueous extract of *Paullinia cupana* leaves, the aqueous solution of $AgNO_3$ and the drug miltefosine (standard drug) were evaluated for cytotoxicity in RAW 264.7 murine macrophages. The CC_{50} values reflecting the cytotoxic concentrations capable of eliminating half of the macrophages are shown in Table 3.

A less prominent cytotoxic effect was observed after exposure to $AgNO_3$, with CC_{50} value of 61.35 µg/

mL, which is close to the values obtained by AgNPs-A (71.48 µg/mL) and AgNPs-M (79.26 µg/mL). The macrophage growth inhibition profile showed improved action when AgNPs-WB, AgNPs-LED, AgNPs-U, and AgNPs-S were used, presenting CC_{50} values of 91.39 µg/mL, 90.4 µg/mL, 83.67 µg/mL, and 164.1 µg/mL, respectively which are close to the cytotoxic concentrations by biogenic AgNPs for J774A.1 macrophages found in previous studies with a CC_{50} value of 116 µg/mL when using *Sargentodoxa cuneata* and CC_{50} of 100.02 µg/mL after exposure of macrophages to AgNPs mediated by *Teucrium stocksianum* extracts [96, 97]. Thus, as indicated by the results described, the AgNPs synthesized through the aqueous extract of a plant native to the Amazon region can be employed in vitro in limited dosages against macrophages, since these are considered the final hosts for the completion of the life cycle of parasites of the species *Leishmania* sp.

The cytotoxicity depends on the physicochemical and morphological characteristics of AgNPs since the particles meet macrophages by endosomal uptake or diffusion. AgNPs can activate macrophages to produce ROS that are capable of inhibiting parasite growth and, in conjunction with this, phytochemicals used as coating and stabilization agents of AgNPs can increase leishmanicidal activity through immunomodulatory effects [98, 99]. Despite their small size and spherical shape, in the present study the AgNPs synthesized via guarana extracts caused low cytotoxicity to host cells, indicating modulation of biological effects and cell selectivity.

The safety of the tested samples was expressed based on the values of the SI, which is the ratio between the cytotoxicity values for host cells (CC_{50}) in relation to the promastigote cells of *Leishmania amazonensis* (IC_{50}), and the results are shown in Table 3. The higher the SI, the better the action against the parasites, affecting to a lesser extent the host cells, thus, AgNPs-U, AgNPs-M, AgNPs-WB, and AgNPs-LED were the samples with the highest selectivity for application against the species of *Leishmania amazonensis* being 14.94, 13.66, 12.93, and 12 times less toxic to RAW 264.7 macrophages, respectively, and having between 0.86 and 1.07 times more selectivity than the drug miltefosine (SI = 13.97).

4 Conclusion

In this study, AgNPs were successfully synthesized using different synthesis routes using plant phytochemicals (phenolic acids, alkaloids, flavonoids) from the aqueous extract of guarana leaves. All the nanostructures, regardless of the equipment/energy source, showed an SPR band within the range considered ideal for AgNPs (420–440 nm), while the colloidal characteristics showed particles with diameters below 100 nm, a surface charge above − 30 mV in the two storage conditions tested, which represents considerable stability and, in turn, the morphology of the AgNPs was predominantly spherical. The evaluation of the antibacterial activity showed the effectiveness of AgNPs in inhibiting the growth of Gram-negative strains *E. coli* and *P. aeruginosa*, as well as the Gram-positive strain *S. aureus*, with the samples obtained using heating-based methods (microwave, ultrasound, and water bath) standing out as having MIC values equal to or lower than those of the aqueous solution of the metal salt (positive control). In relation to the anti-leishmanial tests, our results support evidence that most of the AgNPs tested showed selective action against the promastigote forms of *L. amazonensis*, keeping them safe for the host cells, thus being the first report described on such bioactivity caused by treatment with green nanomaterials using guarana extracts. Thus, it is considered that the AgNPs synthesized from the extract of *Paullinia cupana*, a plant native to Brazilian biodiversity, have potential application in nanomedicine, more precisely by acting as a promising antimicrobial and antileishmanial compound, which may serve to encourage further investigations into research aimed at optimizing the biogenic synthesis of metallic silver nanostructures.

Supplementary Information The online version contains supplementary material available at https://doi.org/10.1007/s13399-023-05250-1.

Acknowledgements This work is based on the doctoral research of the first author of the manuscript and was supported by the Coordenação de Aperfeiçoamento de Pessoal de Nível Superior – Brasil (CAPES), Conselho Nacional de Desenvolvimento Científico e Tecnológico (CNPq) and University of Brasilia (UnB), which provided financial and infrastructure subsidies to carry out the research. The authors are grateful the research institutions listed in the affiliations of each of the co-authors who provided important contributions to the development of this research in terms of the characterization and biological tests of the aqueous plant extract and the synthesized AgNPs, reinforcing the importance of various institutions in building a quality multidisciplinary study. The authors are grateful MSc. Laís Bentes de Almeida and her family for their support and trust in providing from their private property the plant material used in this research. The authors are grateful to Dr. Thaís Elias Almeida for the botanical identification of the plant species.

Author contribution Conceptualization: AKOL, MPG. Methodology: AKOL, APS, RCS, ARA, KAFR, JAAR, CMR. Formal analysis and investigation: APS, RCS, YAAM, ARA, SSMA, JLA, JAAR. Writing—original draft preparation: AKOL, MPG. Writing—review and editing: AKOL, APS, RCS, IRSV, JLA, LCS, KAFR, SWS, JAAR, CMR, MPG. Funding acquisition: MPG. Resources: ARA, KAFR, SWS, CMR, MPG. Supervision: KAFR, SWS, JAAR, CMR, MPG.

Data availability The authors declare that the data supporting the findings of this study are available within the paper.

Declarations

Ethics approval This study did not involve human and/or animal participants and therefore no consent is required for the same.

Conflict of interest The authors declare no competing interests.

References

1. Raj S, Singh H, Trivedi R, Soni V (2020) Biogenic synthesis of AgNPs employing Terminalia arjuna leaf extract and its efficacy towards catalytic degradation of organic dyes. Sci Rep 10(1):9616. https://doi.org/10.1038/s41598-020-66851-8
2. Sibuyi NRS, Moabelo KL, Fadaka AO, Meyer S, Onani MO, Madiehe AM, Meyer M (2021) Multifunctional gold nanoparticles for improved diagnostic and therapeutic applications: a review. Nanoscale Res Lett 16:1–27. https://doi.org/10.1186/s11671-021-03632-w
3. Galúcio JM, de Souza SGB, Vasconcelos AA, Lima AKO, da Costa KS, de Campos BH, Taube PS (2022) Synthesis, characterization, applications, and toxicity of green synthesized nanoparticles. Curr Pharm Biotechnol 23(3):420–443. https://doi.org/10.2174/1389201022666210521102307
4. Hashemi Z, Mohammadyan M, Naderi S, Fakhar M, Biparva P, Akhtari J, Ebrahimzadeh MA (2021) Green synthesis of silver nanoparticles using Ferula persica extract (Fp-NPs): characterization, antibacterial, antileishmanial, and in vitro anticancer activities. Mater Today Commun 27:102264. https://doi.org/10.1016/j.mtcomm.2021.102264
5. Pulit-Prociak J, Grabowska A, Chwastowski J, Majka TM, Banach M (2019) Safety of the application of nanosilver and nanogold in topical cosmetic preparations. Colloids Surf B Biointerfaces 183:110416. https://doi.org/10.1016/j.colsurfb.2019.110416
6. Trieu QA, Le CTB, Pham CM, Bui TH (2023) Photocatalytic degradation of methylene blue and antibacterial activity of silver nanoparticles synthesized from Camellia sinensis leaf extract. J Exp Nanosci 18(1):2225759. https://doi.org/10.1080/17458080.2023.2225759
7. Harish V et al (2022) Nanoparticle and nanostructure synthesis and controlled growth methods. Nanomaterials 12(18):3226. https://doi.org/10.3390/nano12183226
8. Jamkhande PG, Ghule NW, Bamer AH, Kalaskar MG (2019) Metal nanoparticles synthesis: an overview on methods of preparation, advantages and disadvantages, and applications. J Drug Deliv Sci Technol 53:101174. https://doi.org/10.1016/j.jddst.2019.101174
9. Vishwanath R, Negi B (2021) Conventional and green methods of synthesis of silver nanoparticles and their antimicrobial properties. Curr Res Green Sustain Chem 4:100205. https://doi.org/10.1016/j.crgsc.2021.100205
10. Bindhu MR, Umadevi M, Esmail GA, Al-Dhabi NA, Arasu MV (2020) Green synthesis and characterization of silver nanoparticles from Moringa oleifera flower and assessment of antimicrobial and sensing properties. J Photochem Photobiol B Biol 205:111836. https://doi.org/10.1016/j.jphotobiol.2020.111836
11. Li R, Chen Z, Ren N, Wang Y, Wang Y, Yu F (2019) Biosynthesis of silver oxide nanoparticles and their photocatalytic and antimicrobial activity evaluation for wound healing applications in nursing care. J Photochem Photobiol B Biol 199:111593. https://doi.org/10.1016/j.jphotobiol.2019.111593
12. Alayande SO, Akinsiku AA, Akinsipo OB, Ogunjinmi EO, Dare EO (2021) Green synthesized silver nanoparticles and their therapeutic applications. Compr Anal Chem 94:585–611. https://doi.org/10.1016/bs.coac.2021.01.009
13. Raj R, Bhattu M, Verma M, Acevedo R, Duc ND, Singh J (2023) Biogenic silver based nanostructures: synthesis, mechanistic approach and biological applications. Environ Res 116045. https://doi.org/10.1016/j.envres.2023.116045
14. Simon S et al (2022) Biomedical applications of plant extract-synthesized silver nanoparticles. Biomedicines 10(11):2792. https://doi.org/10.3390/biomedicines10112792
15. Schimpl FC, da Silva JF, de Carvalho Gonçalvez JF, Mazzafera P (2013) Guarana: revisiting a highly caffeinated plant from the Amazon. J Ethnopharmacol 150(1):14–31. https://doi.org/10.1016/j.jep.2013.08.023
16. Machado KN et al (2018) A rapid simultaneous determination of methylxanthines and proanthocyanidins in Brazilian guaraná (Paullinia cupana Kunth.). Food Chem 239:180–188. https://doi.org/10.1016/j.foodchem.2017.06.089
17. Mendes TMN et al (2019) Guaraná (Paullinia cupana) catechins and procyanidins: gastrointestinal/colonic bioaccessibility, Caco-2 cell permeability and the impact of macronutrients. J Funct Foods 55:352–361. https://doi.org/10.1016/j.jff.2019.02.026
18. De Oliveira Salles RC, Muniz MP, Nunomura RDCS, Nunomura SM (2022) Geographical origin of guarana seeds from untargeted UHPLC-MS and chemometrics analysis. Food Chem 371:131068. https://doi.org/10.1016/j.foodchem.2021.131068
19. Schimpl FC, Kiyota E, Mayer JLS, de Carvalho Gonçalves JF, da Silva JF, Mazzafera P (2014) Molecular and biochemical characterization of caffeine synthase and purine alkaloid concentration in guarana fruit. Phytochemistry 105:25–36. https://doi.org/10.1016/j.phytochem.2014.04.018
20. Yonekura L et al (2016) Bioavailability of catechins from guaraná (Paullinia cupana) and its effect on antioxidant enzymes and other oxidative stress markers in healthy human subjects. Food Funct 7(7):2970–2978. https://doi.org/10.1039/C6FO00513F
21. Basile A, Rigano D, Conte B, Bruno M, Rosselli S, Sorbo S (2013) Antibacterial and antifungal activities of acetonic extract from Paullinia cupana Mart. seeds. Nat Prod Res 27(22):2084–2090. https://doi.org/10.1080/14786419.2013.784868
22. Antonelli-Ushirobira TM, Kaneshima EN, Gabriel M, Audi EA, Marques LC, Mello JCP (2010) Acute and subchronic toxicological evaluation of the semipurified extract of seeds of guaraná (Paullinia cupana) in rodents. Food Chem Toxicol 48(7):1817–1820. https://doi.org/10.1016/j.fct.2010.04.013
23. Da Costa KC et al (2014) Guaraná, a supplement rich in caffeine and catechin, modulates cytokines: evidence from human in vitro and in vivo protocols. Eur Food Res Technol 239:49–57. https://doi.org/10.1007/s00217-014-2182-3
24. Zeidán-Chuliá F et al (2013) Major components of energy drinks (caffeine, taurine, and guarana) exert cytotoxic effects on human neuronal SH-SY5Y cells by decreasing reactive oxygen species production. Oxid Med Cell Longev 2013. https://doi.org/10.1155/2013/791795
25. Kharissova OV, Kharisov BI, Oliva González CM, Méndez YP, López I (2019) Greener synthesis of chemical compounds and materials. Royal Soc Open Sci 6(11):191378. https://doi.org/10.1098/rsos.191378
26. Doan VD et al (2020) Biosynthesis of silver and gold nanoparticles using aqueous extract of Codonopsis pilosula roots for antibacterial and catalytic applications. J Nanomater 2020:1–18. https://doi.org/10.1155/2020/8492016
27. Vargas LHG et al (2016) Metabolomics analysis of oil palm (Elaeis guineensis) leaf: evaluation of sample preparation steps using UHPLC–MS/MS. Metabolomics 12:1–12. https://doi.org/10.1007/s11306-016-1100-z
28. Ruttkies C, Schymanski EL, Wolf S, Hollender J, Neumann S (2016) MetFrag relaunched: incorporating strategies beyond in silico fragmentation. J Cheminformatics 8(1):1–16. https://doi.org/10.1186/s13321-016-0115-9
29. CLSI Document M7-A7 (2012) Methods for dilution antimicrobial susceptibility tests for bacteria that grow aerobically. Approved Standard. Clinical and Laboratory Standards Institute (CLSI): Wayne, PA, USA 1–76

30 De Lima Nunes TA et al (2021) Eugenia piauhiensis Vellaff. essential oil and γ-elemene its major constituent exhibit antileishmanial activity, promoting cell membrane damage and in vitro immunomodulation. Chem Biol Interact 339:109429. https://doi.org/10.1016/j.cbi.2021.109429

31. Sousa JMSD et al (2023) Cytotoxic and antileishmanial effects of the monoterpene β-ocimene. Pharmaceuticals 16(2):183. https://doi.org/10.3390/ph16020183

32. Hussain M, Raja NI, Iqbal M, Aslam S (2019) Applications of plant flavonoids in the green synthesis of colloidal silver nanoparticles and impacts on human health. Iran J Sci Technol Trans A Sci 43:1381–1392. https://doi.org/10.1007/s40995-017-0431-6

33. Zuhrotun A, Oktaviani DJ, Hasanah AN (2023) Biosynthesis of gold and silver nanoparticles using phytochemical compounds. Molecules 28(7):3240. https://doi.org/10.3390/molecules28073240

34. Karan T, Gonulalan Z, Erenler R, Kolemen U, Eminagaoglu O (2024) Green synthesis of silver nanoparticles using Sambucus ebulus leaves extract: characterization, quantitative analysis of bioactive molecules, antioxidant and antibacterial activities. J Mol Struct 1296:136836. https://doi.org/10.1016/j.molstruc.2023.136836

35. Jain S, Mehata MS (2017) Medicinal plant leaf extract and pure flavonoid mediated green synthesis of silver nanoparticles and their enhanced antibacterial property. Sci Rep 7(1):15867. https://doi.org/10.1038/s41598-017-15724-8

36. Marslin G, Siram K, Maqbool Q, Selvakesavan RK, Kruszka D, Kachlicki P, Franklin G (2018) Secondary metabolites in the green synthesis of metallic nanoparticles. Materials 11(6):940. https://doi.org/10.3390/ma11060940

37. Chahardoli A, Hajmomeni P, Ghowsi M, Qalekhani F, Shokoohinia Y, Fattahi A (2021) Optimization of quercetin-assisted silver nanoparticles synthesis and evaluation of their hemocompatibility, antioxidant, anti-inflammatory, and antibacterial effects. Global Chall 5(12):2100075. https://doi.org/10.1002/gch2.202100075

38. Gröning R, Breitkreutz J, Baroth V, Müller RS (2001) Nanoparticles in plant extracts–factors which influence the formation of nanoparticles in black tea infusions. Pharmazie 56(10):790–792

39. Sahu N, Soni D, Chandrashekhar B, Satpute DB, Saravanadevi S, Sarangi BK, Pandey RA (2016) Synthesis of silver nanoparticles using flavonoids: hesperidin, naringin and diosmin, and their antibacterial effects and cytotoxicity. Int Nano Lett 6:173–181. https://doi.org/10.1007/s40089-016-0184-9

40. Gecer EN, Erenler R (2023) Biogenic synthesis of silver nanoparticles using Echium vulgare: characterisation, quantitative analysis of bioactive compounds, antioxidant activity and catalytic degradation. J Indian Chem Soc 100(5):101003. https://doi.org/10.1016/j.jics.2023.101003

41. Melkamu WW, Bitew LT (2021) Green synthesis of silver nanoparticles using Hagenia abyssinica (Bruce) JF Gmel plant leaf extract and their antibacterial and anti-oxidant activities. Heliyon 7(11). https://doi.org/10.1016/j.heliyon.2021.e08459

42. Shaikh WA, Chakraborty S, Islam RU (2020) Photocatalytic degradation of rhodamine B under UV irradiation using Shorea robusta leaf extract-mediated bio-synthesized silver nanoparticles. Int J Environ Sci Technol 17(4):2059–2072. https://doi.org/10.1007/s13762-019-02473-6

43. Krishnamoorthy K, Jayaraman S, Krishnamoorthy R, Manoharadas S, Alshuniaber MA, Vikas B, Veeraraghavan VP (2023) Green synthesis and evaluation of anti-microbial, antioxidant, anti-inflammatory, and anti-diabetic activities of silver nanoparticles from Argyreia nervosa leaf extract: an invitro study. J King Saud Univ Sci 35(10):102955. https://doi.org/10.1016/j.jksus.2023.102955

44. Jiang XC, Chen WM, Chen CY, Xiong SX, Yu AB (2011) Role of temperature in the growth of silver nanoparticles through a synergetic reduction approach. Nanoscale Res Lett 6:1–9. https://doi.org/10.1007/s11671-010-9780-1

45. Terenteva EA, Apyari VV, Dmitrienko SG, Zolotov YA (2015) Formation of plasmonic silver nanoparticles by flavonoid reduction: a comparative study and application for determination of these substances. Spectrochim Acta A Mol Biomol Spectrsc 151:89–95. https://doi.org/10.1016/j.saa.2015.06.049

46. Ahmed KBA, Senthilnathan R, Megarajan S, Anbazhagan V (2015) Sunlight mediated synthesis of silver nanoparticles using redox phytoprotein and their application in catalysis and colorimetric mercury sensing. J Photochem Photobiol B Biol 151:39–45. https://doi.org/10.1016/j.jphotobiol.2015.07.003

47. Mankad M, Patil G, Patel D, Patel P, Patel A (2020) Comparative studies of sunlight mediated green synthesis of silver nanoparaticles from Azadirachta indica leaf extract and its antibacterial effect on Xanthomonas oryzae pv. oryzae. Arab J Chem 13(1):2865–2872. https://doi.org/10.1016/j.arabjc.2018.07.016

48 Araruna FB et al (2020) Green syntheses of silver nanoparticles using babassu mesocarp starch (Attalea speciosa Mart .ex Spreng.) and their antimicrobial applications. Environ Nanotechnol Monit Manag 13:100281. https://doi.org/10.1016/j.enmm.2019.100281

49. Behravan M, Panahi AH, Naghizadeh A, Ziaee M, Mahdavi R, Mirzapour A (2019) Facile green synthesis of silver nanoparticles using Berberis vulgaris leaf and root aqueous extract and its antibacterial activity. Int J Biol Macromol 124:148–154. https://doi.org/10.1016/j.ijbiomac.2018.11.101

50. Vanlalveni C, Rajkumari K, Biswas A, Adhikari PP, Lalfakzuala R, Rokhum L (2018) Green synthesis of silver nanoparticles using Nostoc linckia and its antimicrobial activity: a novel biological approach. Bionanoscience 8:624–631. https://doi.org/10.1007/s12668-018-0520-9

51. Mohamed N, El-Masry HM (2020) Aloe Vera gel extract and sunlight mediated synthesis of silver nanoparticles with highly effective antibacterial and anticancer activity. J Nanoanalysis 7(1):73–82. https://doi.org/10.22034/jna.2020.1884807.1176

52. Sekar V, Balakrishnan C, Kathirvel P, Swamiappan S, Alshehri MA, Sayed S, Panneerselvam C (2022) Ultra-sonication-enhanced green synthesis of silver nanoparticles using Barleria buxifolia leaf extract and their possible application. Artif Cells Nanomed Biotechnol 50(1):177–187. https://doi.org/10.1080/21691401.2022.2084100

53. Clayton KN, Salameh JW, Wereley ST, Kinzer-Ursem TL (2016) Physical characterization of nanoparticle size and surface modification using particle scattering diffusometry. Biomicrofluidics 10(5). https://doi.org/10.1063/1.4962992

54. Filho ACD et al (2023) Green synthesis silver nanoparticles Bougainvillea glabra Choisy/LED light with high catalytic activity in the removal of methylene blue aqueous solution. Environ Sci Pollut Res 30(13):36244–36258. https://doi.org/10.1007/s11356-022-24633-x

55. Salem MA, Elzwawy A, Elbashar Y, Makram BMA, Abdel-Fattah WI (2023) Feasible microwave-supported silver nanoparticles synthesis by employing sycamore leaves extract, and their characterization. Iran J Sci 1–11. https://doi.org/10.1007/s40995-023-01470-2

56. Meena PR, Singh AP, Tejavath KK (2020) Biosynthesis of silver nanoparticles using Cucumis prophetarum aqueous leaf extract and their antibacterial and antiproliferative activity against cancer cell lines. ACS Omega 5(10):5520. https://doi.org/10.1021/acsomega.0c00155

57. Leroy P, Devau N, Revil A, Bizi M (2013) Influence of surface conductivity on the apparent zeta potential of amorphous silica nanoparticles. J Colloid Interface Sci 410:81–93. https://doi.org/10.1016/j.jcis.2013.08.012

58. Sun Q, Cai X, Li J, Zheng M, Chen Z, Yu CP (2014) Green synthesis of silver nanoparticles using tea leaf extract and evaluation of their stability and antibacterial activity. Colloids Surf A Physicochem Eng Asp 444:226–231. https://doi.org/10.1016/j.colsurfa.2013.12.065
59. De Oliveira Júnior SD et al (2022) Production of lignocellulolytic enzymes and phenolic compounds by Lentinus strigosus from the Amazon using solid-state fermentation (SSF) of guarana (Paullinia cupana) residue. Appl Biochem Biotechnol 194(7):2882–2900. https://doi.org/10.1007/s12010-022-03851-6
60. Kaushik N et al (2020) Antiproliferative activity of pyracantha and Paullinia plant extracts on aggressive breast and hepatocellular carcinoma cells. Appl Sci 10(21):7543. https://doi.org/10.3390/app10217543
61. Dua TK, Giri S, Nandi G, Sahu R, Shaw TK, Paul P (2023) Green synthesis of silver nanoparticles using Eupatorium adenophorum leaf extract: characterizations, antioxidant, antibacterial and photocatalytic activities. Chem Pap 1–10. https://doi.org/10.1007/s11696-023-02676-9
62. Antony A, Farid M (2022) Effect of temperatures on polyphenols during extraction. Appl Sci 12(4):2107. https://doi.org/10.3390/app12042107
63. Bulut O, Yilmaz MD (2022) Quercetagetin-stabilized silver nanoparticles for the oxidation of morin. ACS Appl Nano Mater 5(10):13761–13767. https://doi.org/10.1021/acsanm.2c00834
64. Ansari MJ, Rehman NU, Ibnouf E, Alalaiwe A, Ganaie MA, Zafar A (2022) Gum acacia-and gum tragacanth-coated silver nanoparticles: synthesis, physiological stability, in-vitro, ex-vivo and in-vivo activity evaluations. Coatings 12(10):1579. https://doi.org/10.3390/coatings12101579
65. Shafiq A, Deshmukh AR, AbouAitah K, Kim BS (2023) Green synthesis of controlled shape silver nanostructures and their peroxidase, catalytic degradation, and antibacterial activity. J Funct Biomater 14(6):325. https://doi.org/10.3390/jfb14060325
66. Balaji V et al (2023) Bio-inspired synthesis of silver nanoparticles and their nanocomposites for antibacterial and anticancer activity: a comparative study. J Alloys Compd 966:171503. https://doi.org/10.1016/j.jallcom.2023.171503
67. Yassin MT, Mostafa AAF, Al-Askar AA, Al-Otibi FO (2022) Facile green synthesis of zinc oxide nanoparticles with potential synergistic activity with common antifungal agents against multidrug-resistant candidal strains. Crystals 12(6):774. https://doi.org/10.3390/cryst12060774
68. Khodashenas B, Ghorbani HR (2019) Synthesis of silver nanoparticles with different shapes. Arab J Chem 12(8):1823–1838. https://doi.org/10.1016/j.arabjc.2014.12.014
69. Parit SB et al (2020) Bioinspired synthesis of multifunctional silver nanoparticles for enhanced antimicrobial and catalytic applications with tailored SPR properties. Mater Today Chem 17:100285. https://doi.org/10.1016/j.mtchem.2020.100285
70. Lima AKO, Vasconcelos AA, Kobayashi RKT, Nakazato G, de Campos BH, Taube PS (2021) Green synthesis: characterization and biological activity of silver nanoparticles using aqueous extracts of plants from the Arecaceae family. Acta Sci Technol 43:e52011–e52011. https://doi.org/10.4025/actascitechnol.v43i1.52011
71. Carvalho LVDN et al (2016) Evaluation of antibacterial, antineoplastic, and immunomodulatory activity of Paullinia cupana seeds crude extract and ethyl-acetate fraction. Evid Based Complementary Altern Med 2016. https://doi.org/10.1155/2016/1203274
72. Meikle TG, Dyett BP, Strachan JB, White J, Drummond CJ, Conn CE (2020) Preparation, characterization, and antimicrobial activity of cubosome encapsulated metal nanocrystals. ACS Appl Mater Interfaces 12(6):6944–6954. https://doi.org/10.1021/acsami.9b21783
73. Vijayan R, Joseph S, Mathew B (2018) Indigofera tinctoria leaf extract mediated green synthesis of silver and gold nanoparticles and assessment of their anticancer, antimicrobial, antioxidant and catalytic properties. Artif Cells Nanomed Biotechnol 46(4):861–871. https://doi.org/10.1080/21691401.2017.1345930
74. Erci F, Cakir-Koc R, Isildak I (2018) Green synthesis of silver nanoparticles using Thymbra spicata L. var. spicata (zahter) aqueous leaf extract and evaluation of their morphology-dependent antibacterial and cytotoxic activity. Artif Cells Nanomed Biotechnol 46(sup1):150–158. https://doi.org/10.1080/21691401.2017.1415917
75. Liao C, Li Y, Tjong SC (2019) Bactericidal and cytotoxic properties of silver nanoparticles. Int J Mol 20(2):449. https://doi.org/10.3390/ijms20020449
76. Ahmad SA, Das SS, Khatoon A, Ansari MT, Afzal M, Hasnain MS, Nayak AK (2020) Bactericidal activity of silver nanoparticles: a mechanistic review. Mater Sci Energy Technol 3:756–769. https://doi.org/10.1016/j.mset.2020.09.002
77. Dakal TC, Kumar A, Majumdar RS, Yadav V (2016) Mechanistic basis of antimicrobial actions of silver nanoparticles. Front Microbiol 7:1831. https://doi.org/10.3389/fmicb.2016.01831
78. Silveira AP, Bonatto CC, Lopes CAP, Rivera LMR, Silva LP (2018) Physicochemical characteristics and antibacterial effects of silver nanoparticles produced using the aqueous extract of Ilex paraguariensis. Mater Chem Phys 216:476–484. https://doi.org/10.1016/j.matchemphys.2018.05.068
79 Fayaz AM, Balaji K, Girilal M, Yadav R, Kalaichelvan PT, Venketesan R (2010) Biogenic synthesis of silver nanoparticles and their synergistic effect with antibiotics: a study against gram-positive and gram-negative bacteria. Nanomedicine: Nanotechnol, Biol Med 6(1):103–109. https://doi.org/10.1016/j.nano.2009.04.006
80. Miermont A, Waharte F, Hu S, McClean MN, Bottani S, Léon S, Hersen P (2013) Severe osmotic compression triggers a slowdown of intracellular signaling, which can be explained by molecular crowding. Proc Natl Acad Sci 110(14):5725–5730. https://doi.org/10.1073/pnas.1215367110
81. Mourão MA, Hakim JB, Schnell S (2014) Connecting the dots: the effects of macromolecular crowding on cell physiology. Biophys J 107(12):2761–2766. https://doi.org/10.1016/j.bpj.2014.10.051
82. Rempe CS, Burris KP, Woo HL, Goodrich B, Gosnell DK, Tschaplinski TJ, Stewart CN Jr (2015) Computational ranking of yerba mate small molecules based on their predicted contribution to antibacterial activity against methicillin-resistant Staphylococcus aureus. PLoS One 10(5):e0123925. https://doi.org/10.1371/journal.pone.0123925
83. Dimech GS, Soares LAL, Ferreira MA, de Oliveira AGV, Carvalho MDC, Ximenes EA (2013) Phytochemical and antibacterial investigations of the extracts and fractions from the stem bark of Hymenaea stigonocarpa Mart. ex Hayne and effect on ultrastructure of Staphylococcus aureus induced by hydroalcoholic extract. Sci World J 2013. https://doi.org/10.1155/2013/862763
84. Ullah I, Shinwari ZK, Khalil AT (2017) Investigation of the cytotoxic and antileishmanial effects of Fagonia indica L. extract and extract mediated silver nanoparticles (AgNPs). Pak J Bot 49(4):1561–1568
85. Bezerra TT et al (2022) In vitro antileishmanial activity of sustainable anacardic acid and cardol based silver nanoparticles on L. braziliensis. Int J Pharm 619:121698. https://doi.org/10.1016/j.ijpharm.2022.121698
86. Costa EV et al (2009) Antimicrobial and antileishmanial activity of essential oil from the leaves of Annona foetida (Annonaceae). Quim Nova 32:78–81. https://doi.org/10.1590/S0100-40422009000100015
87. Lima GS, Castro-Pinto DB, Machado GC, Maciel MA, Echevarria A (2015) Antileishmanial activity and trypanothione reductase

effects of terpenes from the Amazonian species Croton cajucara Benth (Euphorbiaceae). Phytomedicine 22(12):1133–1137. https://doi.org/10.1016/j.phymed.2015.08.012
88. Santos AO, Ueda-Nakamura T, Dias Filho BP, Junior VFV, Pinto AC, Nakamura CV (2008) Effect of Brazilian copaiba oils on Leishmania amazonensis. J Ethnopharmacol 120(2):204–208. https://doi.org/10.1016/j.jep.2008.08.007
89. Kalangi SK, Dayakar A, Gangappa D, Sathyavathi R, Maurya RS, Rao DN (2016) Biocompatible silver nanoparticles reduced from Anethum graveolens leaf extract augments the antileishmanial efficacy of miltefosine. Exp Parasitol 170:184–192. https://doi.org/10.1016/j.exppara.2016.09.002
90. Zahir AA et al (2015) Green synthesis of silver and titanium dioxide nanoparticles using Euphorbia prostrata extract shows shift from apoptosis to G0/G1 arrest followed by necrotic cell death in Leishmania donovani. Antimicrob Agents Chemother 59(8):4782–4799. https://doi.org/10.1128/aac.00098-15
91. Olekhnovitch R, Ryffel B, Müller AJ, Bousso P (2014) Collective nitric oxide production provides tissue-wide immunity during Leishmania infection. J Clin Investig 124(4):1711–1722. https://doi.org/10.1172/JCI72058
92. Van Assche T, Deschacht M, da Luz RAI, Maes L, Cos P (2011) Leishmania–macrophage interactions: insights into the redox biology. Free Radic Biol Med 51(2):337–351. https://doi.org/10.1016/j.freeradbiomed.2011.05.011
93. Baiocco P, Ilari A, Ceci P, Orsini S, Gramiccia M, Di Muccio T, Colotti G (2011) Inhibitory effect of silver nanoparticles on trypanothione reductase activity and Leishmania infantum proliferation. ACS Medicinal Chem Lett 2(3):230–233. https://doi.org/10.1021/ml1002629
94. Ilari A et al (2012) A gold-containing drug against parasitic polyamine metabolism: the X-ray structure of trypanothione reductase from Leishmania infantum in complex with auranofin reveals a dual mechanism of enzyme inhibition. Amino Acids 42:803–811. https://doi.org/10.1007/s00726-011-0997-9
95. Kuntz AN, Davioud-Charvet E, Sayed AA, Califf LL, Dessolin J, Arnér ESJ, Williams DL (2007) Thioredoxin glutathione reductase from Schistosoma mansoni: an essential parasite enzyme and a key drug target. PLoS Med 4(6):e206. https://doi.org/10.1371/journal.pmed.0040206
96. Ahmad A, Syed F, Shah A, Khan Z, Tahir K, Khan AU, Yuan Q (2015) Silver and gold nanoparticles from Sargentodoxa cuneata: synthesis, characterization and antileishmanial activity. RSC Adv 5(90):73793–73806. https://doi.org/10.1039/C5RA13206A
97. Ullah I, Cosar G, Abamor ES, Bagirova M, Shinwari ZK, Allahverdiyev AM (2018) Comparative study on the antileishmanial activities of chemically and biologically synthesized silver nanoparticles (AgNPs). 3 Biotech 8:1–8. https://doi.org/10.1007/s13205-018-1121-6
98. Alti D, Veeramohan Rao M, Rao DN, Maurya R, Kalangi SK (2020) Gold–silver bimetallic nanoparticles reduced with herbal leaf extracts induce ROS-mediated death in both promastigote and amastigote stages of Leishmania donovani. ACS Omega 5(26):16238–16245. https://doi.org/10.1021/acsomega.0c02032
99. El-Khadragy M et al (2018) Clinical efficacy associated with enhanced antioxidant enzyme activities of silver nanoparticles biosynthesized using Moringa oleifera leaf extract, against cutaneous leishmaniasis in a murine model of Leishmania major. Int J Environ Res Public Health 15(5):1037. https://doi.org/10.3390/ijerph15051037